Research Square

Preprints are preliminary reports that have not undergone peer review.
They should not be considered conclusive, used to inform clinical practice,
or referenced by the media as validated information.

Optimization of Low-Level Laser Therapy via Skin Stiffness Gradient Analysis Using Optical Coherence Tomography

Chien-Cheng Tai
Taipei Medical University
Gilang Titah Ramadhan
Tiga Serangkai University
Yih-Kuen Jan
University of Illinois Urbana-Champaign
Ben-Yi Liau
Feng Chia University
Sheena Christabel Pravin
Vellore Institute of Technology
Kiruthika Venkataramani
Vellore Institute of Technology
Winson Chiu-Chun Lee
University of Wollongong
Congo Tak Shing Ching
National Chung Hsing University
Chi-Wen Lung
cwlung@asia.edu.tw

Asia University

Article

Keywords: Low-level laser therapy, U-Net, Skin stiffness gradient, Maximum stiffness, Deep learning, optical coherence tomography

Posted Date: September 18th, 2026

DOI: https://doi.org/10.21203/rs.3.rs-9959478/v1

License: This work is licensed under a Creative Commons Attribution 4.0 International License. Read Full License

Additional Declarations: No competing interests reported.

Abstract

Skin stiffness assessment often relies on single maximum values, which may fail to capture the tissue's full mechanical profile. This study presents a personalized evaluation method that uses an optical coherence tomography (OCT) air-jet indentation system integrated with deep learning to analyze stiffness gradients at multiple points. The results demonstrate that 660 nm LLLT for 3 minutes and 808 nm LLLT for 2 minutes yield the most effective tissue responses in terms of stiffness uniformity. These findings highlight the potential of deep learning-enhanced OCT in establishing optimized LLLT protocols, thereby supporting superior clinical outcomes for skin treatments.

Highlights

[1] 660 nm LLLT applied for 3 min and 808 nm LLLT for 2 min yielded the lowest stiffness gradients, indicating optimal biomechanical uniformity across the skin surface.

[2] Shorter exposures favor 808 nm, while 660 nm requires longer durations to achieve comparable structural uniformity.

[3] Deep learning-enhanced OCT with air-jet indentation enables mapping of skin stiffness gradients (a more informative than single maximum stiffness for evaluating LLLT induced tissue remodeling).

Introduction

As the first line of defense, the skin integrates structural barriers with immune responses to prevent infection [1]. Histologically, skin integrity is maintained by a specific layered structure, with the epidermis and its outermost layer, the stratum corneum (SC), being the main focus of protection [2]. While the underlying epidermal layers (e.g., Stratum Basale and Stratum Spinosum) are responsible for continuous cellular regeneration, SC, as a major component of the skin barrier, integrates various cellular elements to maintain water balance and provide defense against environmental factors [3]. Disruption of the integrity of the epidermal layers, whether due to sharp cuts or superficial grazes, drastically alters the microstructural profile and protective function of the skin [4].

To restore these compromised structural barriers, the body initiates skin wound healing, a highly dynamic regenerative process that involves complex interactions between multiple cell types, chemical mediators, and extracellular matrix (ECM) components [5]. Wound healing involves sequential phases of hemostasis, inflammation, proliferation, and remodeling, during which various cell types, cytokines, growth factors, and ECM components work in coordination to restore tissue integrity [6]. During the proliferation phase, fibroblasts migrate to the wound area to synthesize collagen and elastin, which restore tissue tensile strength [7]. This cellular migration process is not random but is guided by mechanical signals from the surrounding microenvironment via a phenomenon known as durotaxis. Durotaxis is a form of directional cell migration in which cells, primarily fibroblasts, move from softer to stiffer ECM [8]. In this mechanism, cells actively sense mechanical cues and tend to move from softer regions of the ECM to stiffer environments. However, failure to maintain a balance between matrix degradation and synthesis often leads to complications, such as chronic wounds that are difficult to heal or the formation of inelastic, hypertrophic scar tissue. Therefore, technological interventions are needed to modulate cellular activity and ensure optimal functional tissue recovery.

Low-level laser therapy (LLLT), also known as photobiomodulation, has attracted widespread attention in regenerative medicine because of its ability to stimulate healing without thermal effects in cells [9, 10]. LLLT uses specific wavelengths of light to modulate cellular pathways, thereby enhancing collagen biosynthesis and accelerating regenerative processes in the skin [11]. The absorption of light energy triggers an increase in mitochondrial membrane potential, oxygen consumption, and adenosine triphosphate (ATP) production [12]. This increase in cellular energy availability accelerates tissue repair in skin wounds.

The therapeutic efficacy of LLLT is primarily governed by the depth of light penetration, which increases with longer wavelengths within the optical window. For instance, while red light (e.g., 660 nm) is predominantly absorbed in the superficial dermis, near-infrared light (808–980 nm) reaches deeper cutaneous and subcutaneous structures. Specifically, 808 nm light has been extensively utilized to modulate deep-seated dermal processes, such as promoting the remodeling of dense collagen fibers in hypertrophic scars and accelerating the healing of deep-tissue injuries [13, 14]. Because of this depth-dependent interaction, the therapeutic protocol—including wavelength, duration, and energy dose—must be precisely tailored to the specific skin layer or condition being targeted. Consequently, LLLT has gained significant traction in clinical dermatology for its ability to non-invasively address both superficial and deep-seated skin pathologies [15].

Red light (630–660 nm) is the most effective wavelength for anti-aging and skin wound healing because of its moderate tissue penetration and stimulation of fibroblasts [16]. LLLT at 660 nm is also beneficial as an adjunct to conventional therapy for treating foot ulcers [17]. The 660 nm wavelength has been extensively studied for its efficacy in promoting wound healing, including incisional and excisional wounds, superficial burns, and DFU [18, 19]. Research indicates that a wavelength of 660 nm enhances angiogenesis, which is crucial for supplying nutrients and oxygen to healing tissues. A study demonstrated that 660 nm laser therapy significantly increased the number of newly formed blood vessels in treated wounds compared to controls [20]. This proangiogenic effect is vital for tissue regeneration and repair. Additionally, 660 nm LLLT has been shown to stimulate fibroblast proliferation and collagen synthesis [21].

Mechanical characterization of tissue stiffness (e.g., skin in our case) is essential to understanding how different regions within a wound may respond to therapy [22]. Techniques such as ultrasound elastography, magnetic resonance elastography (MRE), and optical coherence elastography (OCE) enable non-invasive mapping of mechanical properties that quantify stiffness [23–25]. Ultrasound shear wave elastography, which has been widely studied in dermatology, provides real-time stiffness imaging and reliably discriminates between scarred and healthy skin regions [25]. Optical coherence elastography offers sub-millimeter resolution and depth-resolved elasticity measurements across skin layers, including the epidermis and dermis, making it particularly valuable for high-granularity stiffness mapping [23]. In vitro and ex vivo studies have further shown that stiffness gradients engineered into ECM hydrogels strongly influence fibroblast morphology, alignment, and migration, underscoring the importance of mapping spatial stiffness variability.

The presence of stiffness gradients in healing tissues has been shown to direct key cellular behaviors, such as duro-taxis-mediated fibroblast and endothelial migration toward stiffer regions, which facilitates granulation tissue formation and re-epithelialization [8]. Computational mechanobiology models of skin repair further reinforce that these mechanical gradients not only correlate with collagen deposition and wound contraction but also govern the risk of fibrotic scarring. When these gradients are excessively steep or non-uniformly distributed, they can trigger aberrant fibroblast activation and persistent myofibroblast differentiation, leading to hypertrophic scars. Additionally, studies of engineered biomaterials have demonstrated that incorporating stiffness gradients within hydrogels can modulate the expression of inflammatory mediators (e.g., IL-10, COX-2). These studies reveal that cells are sensitive to the steepness of the mechanical gradient rather than just absolute stiffness, which dictates the transition toward a pro-healing phenotype. Taken together, these findings suggest that mapping the complexity of stiffness gradients, rather than relying on global average values, is essential to reveal distinct mechanical zones and transition areas within a wound that are either more receptive to therapy or prone to fibrosis.

Despite the known effects of LLLT on cellular metabolism, how specific laser parameters, namely wavelength and exposure duration, collectively modulate the spatial mechanical environment of the skin remains poorly understood. The research question driving this study is whether different LLLT protocols can precisely alter skin stiffness and, more importantly, the resulting stiffness gradients that govern tissue regeneration. We hypothesized that the interaction between laser wavelength and duration would significantly influence the stiffness gradient of the cutaneous tissue. Specifically, we anticipated that certain combinations may yield distinct gradients, where an abrupt mechanical transition (a high stiffness gradient) could potentially compromise structural integrity, whereas a more homogenous distribution would be conducive to optimal functional recovery. In this context, a 'suitable' LLLT protocol is defined as one that maintains low stiffness gradients to ensure long-term tissue flexibility. To test this, a deep learning-based segmentation model was implemented to delineate the epidermal layers with high precision. This computational approach enabled the systematic extraction of localized mechanical data, allowing for a robust assessment of how LLLT-induced stiffness gradients can be optimized to support healthy skin biomechanics.

Result

The results regarding the effect of laser wavelength on maximum stiffness showed no significant differences. Skin stiffness gradients indicated that the 2 min LLLT at 660 nm was significantly higher than that at 808 nm (0.21 ± 0.05 vs. 0.08 ± 0.01, *P* = 0.034), as shown in Table 1, Fig. 2A, and Fig. 2C.

Table 1
Effect of laser wavelength on skin stiffness gradient.

Parameter	Laser duration	Laser Wavelength		Paired t-test
		660 nm (Mean ± SE)	808 nm (Mean ± SE)	*P* value
Maximum Stiffness (N/mm)	2 min	1.71 ± 0.24	1.49 ± 0.15	0.358
	3 min	1.71 ± 0.26	1.07 ± 0.13	0.065
	5 min	1.28 ± 0.13	1.28 ± 0.11	0.995
Stiffness Gradient (N/mm^2)	2 min	0.21 ± 0.05	0.08 ± 0.01	**0.034** *
	3 min	0.10 ± 0.02	0.12 ± 0.02	0.667
	5 min	0.13 ± 0.02	0.19 ± 0.05	0.766
Note: Data are the mean ± standard error; * significant difference (P < 0.05); N, Newton; mm, millimeter.				

The results for the effect of laser duration on maximum stiffness at 660 nm showed a significant difference between 2 min and 3 min (1.49 ± 0.15 vs. 1.07 ± 0.13, P = 0.032). Additionally, skin stiffness gradients indicated that the 660 nm wavelength showed a significant difference at 2 min compared with 3 min (0.21 ± 0.05 vs. 0.10 ± 0.02, P = 0.034). At 808 nm, LLLT for 5 min was significantly higher than that for 2 min (0.08 ± 0.01 vs.

0.12 ± 0.02, P = 0.019), as shown in Table 2, Fig. 2B, and Fig. 2D. An illustration of a low skin stiffness gradient is shown in Fig. 2E, and that of a high skin stiffness gradient is shown in Fig. 2F.

Table 2
Effect of laser duration on stiffness gradient.

Parameter	Wavelength	LLLT Duration									One-way ANOVA	LSD Post hoc			
		2 min (Mean ± SE)			3 min (Mean ± SE)			5 min (Mean ± SE)			P value		2 min vs. 3 min	2 min vs. 5 min	3 min vs. 5 min
Stiffness Maximum (N/mm)	660 nm	1.71	±	0.24	1.71	±	0.26	1.28	±	0.13	0.292	0.996		0.175	0.176
	808 nm	1.49	±	0.15	1.07	±	0.13	1.28	±	0.11	0.096	**0.032**	*	0.277	0.265
Stiffness Gradient (N/mm^2)	660 nm	0.21	±	0.05	0.10	±	0.02	0.13	±	0.02	0.088	**0.034**	*	0.117	0.544
	808 nm	0.08	±	0.01	0.12	±	0.02	0.19	±	0.05	0.056	0.357		**0.019**	* 0.129

Note: Data are presented as mean ± standard error; *, significant difference (P < 0.05); N, Newton; mm, millimeter.

Discussion

This study investigated the effects of laser wavelength and LLLT duration on skin stiffness and stiffness gradients. Although the maximum stiffness values did not differ significantly across conditions, the analysis of skin stiffness gradients revealed distinct mechanical responses. Specifically, at a 2 min duration, the 660 nm wavelength produced a significantly stiffer gradient than the 808 nm wavelength. Furthermore, the duration of exposure played a critical role in a wavelength-dependent manner: for the 660 nm laser, a 2 min application produced significantly higher gradients than a 3 min application, whereas for the 808 nm laser, a 5 min application produced significantly higher gradients than a 2 min application. These findings suggest that although the maximum stiffness after LLLT may not differ, the gradient does. The 660 nm wavelength appears more effective at generating high stiffness gradients during shorter exposure times, whereas the 808 nm wavelength requires longer exposure times to achieve a comparable mechanical effect. This suggests that the interplay between wavelength and duration is a key determinant of localized mechanical remodeling of the skin, with 2 min of 660 nm LLLT producing the most pronounced effect on gradient formation.

The experimental results demonstrate a clear divergence in the temporal response of skin stiffness between the two wavelengths, highlighting the importance of optimizing exposure time. 808 nm near-infrared light reaches the optimal therapeutic window for structural remodeling faster than 660 nm red light [26]. The 808 nm light establishes a homogeneous biomechanical response across the skin grid much earlier than the 660 nm light, which initially creates high-intensity but localized stiffness that requires more time to diffuse and equilibrate [27]. Red light at 660 nm primarily affects the superficial skin layers, such as the epidermis and upper dermis, owing to its limited penetration depth of approximately 1–2 mm. In contrast, near-infrared light at 808 nm penetrates deeper, reaching the dermis and subcutaneous tissues to depths of 4–5 mm. This deeper penetration allows 808 nm light to influence a broader range of skin structures within the same exposure time [28]. The effects of LLLT are mediated through light absorption by mitochondrial chromophores, particularly cytochrome c oxidase (CCO). This absorption enhances mitochondrial respiration and ATP production, promoting cellular activities such as proliferation and tissue repair. Studies have demonstrated that 808 nm irradiation can significantly enhance ATP production in human neuronal cells [29]. While 660 nm light also stimulates ATP production, its effects are more confined to the superficial layers, potentially resulting in less uniform tissue responses when applied for shorter durations. When applying LLLT for 2 min, the limited penetration of 660 nm light may lead to uneven stimulation across skin layers, affecting only superficial tissues and leaving deeper structures unaltered. This can result in a higher stiffness gradient due to differences in tissue responses. Conversely, the deeper penetration of 808 nm light allows for more uniform stimulation of superficial and deeper skin layers within the same timeframe, leading to a more homogeneous tissue response and a lower stiffness gradient. Therefore, for short-duration LLLT aimed at reducing the skin stiffness gradient, 808 nm may be more effective than 660 nm LLLT, as illustrated in Fig. 3A.

The response of skin tissue to LLLT at 660 nm is dose-dependent and follows the Arndt-Schulz law, or the biphasic dose-response, which states that low doses stimulate. In contrast, higher doses may inhibit or reverse the therapeutic effects [30]. When 660 nm was applied for 3 min, it delivered an optimal energy dose (fluence) that sufficiently activated mitochondrial processes across the superficial and upper dermal layers, which is suitable for wound healing because the wound covers the skin layer and disrupts the structure in the upper layer of the skin. This leads to more uniform collagen softening, improved microcirculation, and a reduced stiffness gradient. Skin stiffness is influenced not only by collagen structure but also by the hemodynamic status of the tissue. External pressure regulation has been shown to modulate microcirculation in healthy participants [31], suggesting a complex interaction between mechanical loading and physiological skin responses, as observed in our OCT

measurements. However, extending the exposure to 5 min may exceed the optimal photobiomodulation threshold, potentially leading to accumulation of reactive oxygen species (ROS) or photoinhibition in superficial cells [32]. This can lead to cellular fatigue or inflammation, reducing uniformity in the skin's mechanical response and thereby increasing the stiffness gradient compared to the 3 min treatment.

When 808 nm near-infrared light is applied for 2 min, the energy penetrates deeply into the dermis and subcutaneous layers, efficiently stimulating fibroblast activity, collagen remodeling, and microvascular perfusion [33]. This effect produces uniform softening across deeper tissue structures, correlating with a lower overall stiffness gradient measured post-LLLT. Deeper energy deposition at this wavelength allows metabolic activation and structural remodeling, even within a short timeframe, promoting biomechanical uniformity without overstimulation [34]. However, extending the exposure to 3 min can push the tissue beyond the optimal therapeutic window, as illustrated in Fig. 3B and Fig. 3C. Although additional energy is delivered, deeper tissues may experience nonuniform softening, localized heating, or cellular overstimulation, especially in regions with variable perfusion or metabolic capacity [35]. These imbalances can manifest as an elevated stiffness gradient, reflecting inconsistent mechanical responses across skin layers. Studies have shown that prolonged exposure to 808 nm radiation, even at moderate fluences, can trigger imbalanced reactive oxygen species generation or thermal activation, mildly inhibiting portions of the tissue [36]. Further extending the 808 nm irradiation to 5 min further intensified these disparities. Deeper layers may accumulate heat or oxidative stress owing to prolonged photon absorption, whereas shallower regions may plateau in their response. This combination leads to a high thermal load, cellular fatigue, and a higher stiffness gradient, indicating diminished uniform mechanical improvement. Findings from in vitro studies suggest that high-fluence or extended NIR exposure can elevate reactive oxygen species levels and stress signaling, thereby reducing therapeutic efficacy [36]. These results highlight the critical need to optimize the duration when using deep-penetrating wavelengths, such as 808 nm, to avoid overstimulation and ensure consistent biomechanical outcomes.

Although this study provides empirical data on the biomechanical effects of low-level laser therapy (LLLT), several limitations must be addressed. First, this study was conducted exclusively on healthy skin. The biochemical environment of a wound involves complex inflammatory and cellular dynamics that differ significantly from those in healthy tissue [37]. Future studies should validate these findings using wound environments. Second, a pulse laser was not used in this research, which limits the findings to continuous-wave interactions. Rapid thermal cycling is inherent in pulsed lasers and affects the material's microstructural integrity and thermal relaxation. This is because pulsing can significantly increase material stiffness, as demonstrated in previous studies [38]. Comparing pulsed with continuous lasers will optimize the comprehensiveness of laser–material processing. Third, the measurements were taken immediately following the intervention, failing to account for the long-term or cumulative effects of repeated LLLT sessions [39]. The biological response to LLLT often involves delayed signaling pathways and protein synthesis that may not be fully evident in the acute phase. This is because photobiomodulation triggers sustained cellular changes that accumulate over multiple exposures rather than as a single event.

This study confirms that LLLT intervention significantly modulates the biomechanical characteristics of the skin, particularly by regulating the stiffness gradient. Empirical data from precise OCT observations identified two optimal protocols: 808 nm laser exposure for 2 min and 660 nm laser exposure for 3 min. These specific parameters yielded the lowest stiffness gradients alongside the highest maximum stiffness values, indicating a significant increase in skin stiffness across a broader surface area rather than isolated points.

This reduction in the stiffness gradient indicates increased structural uniformity in the epidermis and stratum corneum, which is clinically crucial for minimizing mechanical stress concentrations. Optimizing these laser parameters offers significant potential for developing regenerative therapy protocols that focus not only on the speed of wound closure but also on restoring the tissue's biomechanical properties to their original physiological condition. Furthermore, these findings provide empirical evidence that the effectiveness of photobiomodulation depends not only on the exposure duration. By achieving greater mechanical uniformity, the skin's functional integrity can be improved.

Methods

1. Participants

This study employed a within-subject, repeated-measures design. Each participant underwent all six LLLT protocols in a single-arm exploratory framework. To ensure the accuracy of the biomechanical measurements, specific inclusion and exclusion criteria were established. Participants were eligible if they were healthy adults aged 19–40 years with intact skin and no history of chronic skin diseases (e.g., psoriasis or eczema) or systemic conditions affecting connective tissues [40]. The age limit was set to minimize age-related variations in skin elasticity [41]. Exclusion criteria included the presence of scars, tattoos, or active skin injuries at the measurement sites to avoid data artifacts [42]. Furthermore, current smokers and regular alcohol consumers were excluded, as these factors are known to increase skin stiffness through collagen degradation [43]. Participants were also prohibited from using topical creams or medications 48 hours before testing to maintain natural skin hydration [44].

The study involved 16 healthy participants (five men and 11 women) aged 19–40 years, with participant characteristics (mean ± SD) showing an age of 27.1 ± 7.2 years, body weight of 57.5 ± 16.8 kg, height of 162.3 ± 8.3 cm, and body mass index (BMI) of 21.9 ± 7.5 kg/m2. All measurements were conducted in a controlled environment with a room temperature of 24 ± 2°C, as temperature significantly influences skin stiffness and tissue relaxation [45]. The Central Regional Research Ethics Committee approved this study at the China Medical University, Taichung, Taiwan (CRREC-

112-130/2) and and subse-quently registered in the International Trial Registry since 2026-07-02 [ClinicalTrials.gov: Identifier NCT07680309 (https://clinicaltrials.gov/study/NCT07680309)]. As a prerequisite for participation in the study, all participants received information about its purpose and procedures. All participants provided written informed consent. The participants were assured that their data would be kept confidential. The responses were anonymized, and a confidentiality agreement was established, allowing respondents to withdraw from the study at any time, in accordance with the Declaration of Helsinki [46].

2. Equipments

The measurement of skin stiffness was performed using a custom-integrated OCT–air jet indentation system. This system employs a non-contact approach to assess tissue deformation in response to controlled air pressure, providing high-resolution tomographic insights into the structural integrity of the skin.

A high-speed OCT device (OPXSV1-02F; OPXION Tech. Inc., New Taipei City, Taiwan) served as the imaging core, featuring a super-luminescent diode light source with a central wavelength of 1,310 nm and an output power of 5 mW. The system achieved a vertical optical resolution of 7.5 μm, a horizontal resolution of 10 μm, and an imaging depth of approximately 2 mm in scattering tissues. Data acquisition was managed via specialized software (OPXION Imaging System V1.0) hosted on a high-performance workstation (ASUS ROG, Taiwan) at a frame rate of 25 Hz.

To induce localized mechanical deformation, a controlled air pulse was generated using a 40 PSI, 22 LPM air compressor (UNi-CROWN Co., Ltd., New Taipei City, Taiwan) connected to a 2 mm positive-pressure port on the OCT probe. This non-contact indentation mechanism is crucial for two reasons: first, it eliminates the risk of cross-infection in compromised skin and second, it prevents the artificial alteration of stiffness measurements that typically occurs when a physical probe pre-loads the skin [47], thereby ensuring that the tissue remains in its natural resting state during assessment. The resulting dynamic displacement of the skin layers was captured by the OCT system to enable the subsequent calculation of the skin stiffness gradient.

An electronic proportional valve (ITV 1030-311L-Q, SMC Corporation, Tokyo, Japan) with pressure feedback and a measuring range of 0.5 MPa was used between the air compressor and the OCT device. The OCT-air-jet indentation system is illustrated in Fig. 1A and Fig. 1B illustrates the mechanism of the OCT-air-jet indentation system and highlights the role of the valve in controlling the pressure for stiffness evaluation.

The intervention used a red dot laser diode module, Class IIIA (TIM201, 660 ± 10 nm, output 80 ± 10 mW, Transverse Industries Co., Ltd., New Taipei, Taiwan). This device emits coherent red light at 660 nm and near-infrared light at 808 nm. The Class IIIA classification indicates that the laser operates with an output power between 1 and 5 mW, making it suitable for therapeutic applications while maintaining safety standards. The laser module design ensures a stable, focused beam, facilitating the precise targeting of the wound area without thermal damage to the surrounding tissues.

3. Experimental Procedure

The experimental measurements were conducted on the palmar surface. The palm was selected for this study due to its significantly thicker stratum corneum, which enhances the contrast needed to clearly visualize distinct skin layers in OCT images [48]. Prior to any measurements, the participants underwent a stabilization period in which they were instructed to rest their hand comfortably for 10 min. This crucial step minimized the influence of recent physical activity or environmental stressors on skin properties, ensuring a stable baseline [49]. Subsequently, a 3×3 grid with 1 cm vertical and horizontal spacing was drawn to define a consistent set of measurement points, as shown in Fig. 1C. The OCT probe was then rigidly mounted and positioned to remain perpendicular to the skin surface (90°), maintaining a precise non-contact distance of 5 mm throughout data acquisition. Each measurement at a single point lasted for a total of 15 sec, as illustrated in Fig. 1D, and was strategically segmented into three distinct 5 sec phases: an initial pre-stimulation phase with the air pressure valve closed, a central stimulation phase in which the valve was opened to apply air pressure to the skin, and a final post-stimulation phase following the valve was closed again. The central segment of each OCT image was extracted to evaluate the peak skin displacement. No sham control condition was included in this exploratory study. Before LLLT was applied, skin measurement served as the within-subject baseline for each protocol.

After baseline measurements were obtained, LLLT intervention was applied directly to the grid-marked area of the palm. Six distinct LLLT protocols were employed in a structured manner to investigate the parameter-dependent effects of photobiomodulation, combining 660 nm and 808 nm wavelengths and application times of 2, 3, and 5 min [50]. Resulting in the following conditions: 1) 660 nm for 2 min, 2) 660 nm for 3 min, 3) 660 nm for 5 min, 4) 808 nm for 2 min, 5) 808 nm for 3 min, and 6) 808 nm for 5 min. The order of the six LLLT protocols was randomized across participants to prevent anticipatory bias. Immediately following LLLT application, post-intervention stiffness measurements (after LLLT) were taken by repeating the identical 15 sec data acquisition protocol at all nine original grid points. This allowed for a direct comparison of the pre- and post-treatment stiffness values under consistent conditions, as this protocol consisted of a single measurement session per participant per day, with a 24 h washout period enforced before any participant could be tested with a different protocol. This precaution was essential because LLLT is known to induce a transient neural blockade and inhibit action potentials in peripheral nerves, an effect that typically reverses

within approximately 24 h [51]. No amendments to the trial protocol were made after commencement. All outcomes reported were prespecified prior to data collection. Adverse events were monitored throughout each session by visual inspection of the measurement site and participant self-report. No thermal or mechanical harm was anticipated given the non-contact nature of the OCT–air jet system and the Class IIIA laser classification.

4. Data Analysis

Skin layer segmentation was performed using a U-Net-based deep learning model. The U-Net architecture was selected for its specialized symmetric structure, which combines a contracting path to capture global context and an expanding symmetric path to enable precise localization [52]. This dual-path mechanism is particularly effective for Optical Coherence Tomography (OCT) scans, where the boundaries between thin layers, such as the stratum corneum and viable epidermis, are often characterized by low contrast or speckle noise [53]. Compared to standard convolutional neural networks, the U-Net requires fewer training samples to achieve high segmentation accuracy, making it ideal for specialized medical datasets [54]. This segmentation process provided the coordinates necessary for localized stiffness measurements as shown in Fig. 1E. In this study, a pre-trained U-Net model was employed to segment the stratum corneum (SC), which served as the reference structure for quantifying skin deformation during OCT–air jet indentation. The model was trained on 560 manually annotated OCT images, with 140 images reserved as a holdout test set to evaluate model generalizability and segmentation performance. To ensure balanced representation and minimize subject-specific bias, every 20 images in the dataset were obtained from a single participant. The trained model achieved an accuracy of 92% in SC segmentation. All computational processes were performed using MATLAB 2024b (The MathWorks, Natick, MA, USA).

Following data acquisition, the raw OCT images were processed to quantify skin deformation over time. At each measurement location, OCT images were acquired for 15 sec, producing a sequence of frames capturing the skin's dynamic response to air-jet loading. The central column of pixels from each frame was extracted and concatenated to form a data matrix representing the complete displacement profile of the skin surface. This procedure produced a composite dataset consisting of 150 columns per measurement location, corresponding to the temporal sequence of skin movement.

The pre-trained U-Net model was applied to each frame to automatically segment the SC layer, thereby enabling precise tracking of its vertical displacement over the 15 sec measurement period. The deformation dynamics of the segmented SC layer under the applied air pressure were subsequently used to compute the local skin stiffness for each dataset. Skin stiffness was calculated using Eq. 1.

$$K = \frac{F}{\Delta d} \text{ [1]}$$

The stiffness parameter (K) is defined as the ratio of the applied force (F) to the skin displacement (Δd). F represents the applied force, which is determined by multiplying the air-jet pressure by the tube area, whereas Δd denotes skin movement.

Once stiffness values were obtained for all nine locations under both pre- and post-LLLT conditions, a spatial analysis was performed. To achieve a more granular representation of the mechanical landscape, the initial 3 × 3 stiffness matrix was refined by integrating additional nodes. The primary objective of this analysis was to identify the direction and magnitude of the greatest stiffness change across the palm. This was achieved by calculating the spatial gradient of the stiffness values across the grid. From this gradient field, the maximum change in gradient was identified and extracted for each participant under each condition (before and after LLLT). These maximum gradient values, representing the most pronounced local stiffness variation, served as the key dependent variables for subsequent statistical analysis to evaluate the significant effects of the LLLT intervention, as illustrated in Fig. 1F.

The stiffness gradient was calculated as the minimum pressure gradient between adjacent locations within the rows and columns. The stiffness values in the horizontal and vertical directions can be calculated using Equations (2) and (3), respectively.

$$Gx\,(i,j) = \frac{K(i+1,\,j)-K(i,j)}{\Delta d} \text{ [2]}$$

$$Gy\,(i,j) = \frac{K(i,\,j+1)-K(i,j)}{\Delta d} \text{ [3]}$$

To further analyze the stiffness variation, the magnitude of the stiffness gradient was computed using the Euclidean norm, which quantifies the overall change in stiffness in both the horizontal and vertical directions. The magnitude is expressed in Eq. (4), where cap $Gx\,(i,j)$ and $Gy\,(i,j)$n represents the stiffness differences along the horizontal and vertical axes, respectively.

$$Magnitude = \sqrt{Gx^2 + Gy^2} \text{ [4]}$$

5. Statistical Analysis

All 16 enrolled participants successfully completed all six LLLT protocols across the full measurement schedule, resulting in a complete dataset with no missing values. No participant withdrew from the study, was lost to follow-up, or was excluded from analysis due to protocol deviation or equipment failure. The stiffness gradient values are reported as the mean ± standard error. A one-way analysis of variance (ANOVA), followed by the least significant difference (LSD) post hoc test, was conducted to evaluate the effect of laser duration across exposure times of 2, 3, and 5 min. Paired t-tests were used to compare LLLT wavelength variations (660 nm vs. 808 nm) in stiffness gradient measurements. All statistical analyses were conducted using SPSS version 22 (IBM, NY, USA) with a significance level of 0.05. No subgroup or sensitivity analyses were prespecified or conducted.

Declarations

Acknowledgment

The authors express gratitude to Dr. Wei-Cheng Shen, Mrs. Yori Pusparani, Ms. Ardha Ardea Prisilla, Ms. Maftuhah Rahimah Rum, Ms. Mariya Nissar, and Mrs. Sylvatera Ayu Puspitasari for their assistance.

Author contributions

Conceptualization, Y.-K.J. and C.-W.L.;

Methodology: C.-C.T., and G.T.R.;

Validation: B.-Y.L., S.C.P., K.V., W.C.-C.L., and C.T.-S.C.;

Writing—original draft: C.-C.T. and G.T.R.;

Writing—review and editing: Y.-K.J. and C.-W.L.;

All authors have read and agreed to the published version of the manuscript.

Data availability statement

The data supporting the conclusions of this article will be made available by the authors, without undue reservation.

Competing Interest

The authors declare that they have no affiliations with or involvement in any organization or entity with any financial interest in the subject matter or materials discussed in this manuscript.

Funding Statement

This study was supported by grants from the National Science and Technology Council of Taiwan (NSTC 114-2923-E-468-001-MY3 and NSTC 114-2410-H-468-016). The funding agency was not involved in the data collection, analysis, or interpretation.

Ethical Experimentation: The studies involving humans were approved by Central Regional Research Ethics Committee China Medical University, Taichung, Taiwan (CRREC-112-130/2). The studies were conducted in accordance with the local legislation and institutional requirements. The participants provided their written informed consent to participate in this study.

Article type statement: This study is classified as a preliminary experimental study. This study was registered in the International Trial Registry [ClinicalTrials.gov: Identifier NCT07177274]

References

1. McKnight, G., Shah, J. & Hargest, R. Physiology of the skin. *Surg. (Oxford)*. **40** (1), 8–12 (2022).
2. de Szalay, S. & Wertz, P. W. Protective Barriers Provided by the Epidermis. *Int. J. Mol. Sci.* **24** (4), 3145 (2023).
3. Jiao, Q. et al. Studies on stratum corneum metabolism: function, molecular mechanism and influencing factors. *J. Cosmet. Dermatol.* **21** (8), 3256–3264 (2022).
4. Chopra, H. et al. Wound dressings: Recent updates. *Int. J. Surg.* **104**, 106793 (2022).

5. Potekaev, N. N. et al. The role of extracellular matrix in skin wound healing. *J. Clin. Med.* **10** (24), 5947 (2021).
6. Yang, F. et al. The Biological Processes During Wound Healing. *Regen. Med.* **16** (4), 373–390 (2021).
7. Gardeazabal, L. & Izeta, A. Elastin and collagen fibres in cutaneous wound healing. *Exp. Dermatol.* **33** (3), e15052 (2024).
8. Espina, J. A., Marchant, C. L. & Barriga, E. H. Durotaxis: the mechanical control of directed cell migration. *FEBS J.* **289** (10), 2736–2754 (2022).
9. Farivar, S., Malekshahabi, T. & Shiari, R. Biological effects of low level laser therapy. *J. Lasers Med. Sci.* **5** (2), 58–62 (2014).
10. Liu, J. et al. Effects of Near Infrared Light on Surgical Wound Healing: A Systematic Review and Meta-Analysis. *Int. Wound J.* **23** (2), e70841 (2026).
11. Avci, P. et al. *Low-level laser (light) therapy (LLLT) in skin: stimulating, healing, restoring*. in *Seminars in cutaneous medicine and surgery*. (2013).
12. Ferraresi, C. et al. *Low-level laser (light) therapy increases mitochondrial membrane potential and ATP synthesis in C2C12 myotubes with a peak response at 3–6 h.* Photochemistry and photobiology, 91(2): pp. 411–416. (2015).
13. Freitas, C. P. et al. Efficacy of low-level laser therapy on scar tissue. *J. Cosmet. Laser Therapy*. **15** (3), 171–176 (2013).
14. Wan, Z. et al. NIR light-assisted phototherapies for bone-related diseases and bone tissue regeneration: A systematic review. *Theranostics* **10** (25), 11837 (2020).
15. Cheng, Y. C. et al. Evaluating the Far-Infrared Radiation Bioeffects on Micro Vascular Dysfunction, Nervous System, and Plantar Pressure in Diabetes Mellitus. *Int. J. Low Extrem Wounds*. **19** (2), 125–131 (2020).
16. Chang, H. et al. Red light promotes dermis-epidermis remodeling via TGFβ and AKT-mediated collagen dynamics in naturally aging mice. *Zoological Res.* **46** (5), 967 (2025).
17. Mathur, R. et al. Low-level laser therapy as an adjunct to conventional therapy in the treatment of diabetic foot ulcers. *Lasers Med. Sci.* **32** (2), 275–282 (2017).
18. Do Nascimento, P. M. et al. A preliminary report on the effect of laser therapy on the healing of cutaneous surgical wounds as a consequence of an inversely proportional relationship between wavelength and intensity: histological study in rats. *Photomed. Laser Surg.* **22** (6), 513–518 (2004).
19. Chen, Q. et al. Optimization of photo-biomodulation therapy for wound healing of diabetic foot ulcers in vitro and in vivo. *Biomedical Opt. Express*. **13** (4), 2450–2466 (2022).
20. Colombo, F. et al. Effect of low-level laser therapy (λ660 nm) on angiogenesis in wound healing: a immunohistochemical study in a rodent model. *Braz. Dent. J.* **24** (4), 308–312 (2013).
21. Ma, H. et al. Effect of low-level laser therapy on proliferation and collagen synthesis of human fibroblasts in vitro. *J. wound Manage. Res.* **14** (1), 1–6 (2018).
22. Guimarães, C. F. et al. The stiffness of living tissues and its implications for tissue engineering. *Nat. Reviews Mater.* **5** (5), 351–370 (2020).
23. Singh, M. et al. Optical coherence elastography. *Nat. Reviews Methods Primers*. **5** (1), 39 (2025).
24. Sack, I. Magnetic resonance elastography from fundamental soft-tissue mechanics to diagnostic imaging. *Nat. Reviews Phys.* **5** (1), 25–42 (2023).
25. Miller, T. et al. Using ultrasound elastography to assess non-invasive, non-pharmacological interventions for musculoskeletal stiffness: a systematic review and meta-analysis. *Disabil. Rehabil.* **46** (16), 3549–3563 (2024).
26. Kuamoto, J. N. et al. Comparison of the effects of laser photobiomodulation at wavelength of 660 nm and 808 nm in full-thickness burns in rats: a pre-clinical study. *Lasers Med. Sci.* **40** (1), 136 (2025).
27. Sleep, S. et al. Assessment of the influence of 660 and 808-nm PBM treatments on mitochondrial oxygen consumption of MG-63 osteoblast: a 3D cell culture study. *Lasers Med. Sci.* **40** (1), 84 (2025).
28. Al-Halawani, R., Qassem, M. & Kyriacou, P. A. Monte Carlo simulation of the effect of melanin concentration on light-tissue interactions in transmittance and reflectance finger photoplethysmography. *Sci. Rep.* **14** (1), 8145 (2024).
29. Oron, U. et al. Ga-As (808 nm) laser irradiation enhances ATP production in human neuronal cells in culture. *Photomed. Laser Surg.* **25** (3), 180–182 (2007).
30. Huang, Y. Y. et al. Biphasic dose response in low level light therapy - an update. *Dose Response*. **9** (4), 602–618 (2011).
31. Ramadhan, G. T. et al. Exploring air insole pressure and walking durations effects on microcirculation in healthy individuals to optimize diabetic foot ulcers prevention. *Sci. Rep.* **15** (1), 10603 (2025).
32. Mathioudaki, E. et al. Photobiomodulation and Wound Healing: Low-Level Laser Therapy at 661 nm in a Scratch Assay Keratinocyte Model. *Ann. Biomed. Eng.* **52** (2), 376–385 (2024).
33. Felician, M. C. P. et al. Photobiomodulation: Cellular, molecular, and clinical aspects. *J. Photochem. Photobiology*. **17**, 100197 (2023).
34. Lyu, K. et al. The Functions and Mechanisms of Low-Level Laser Therapy in Tendon Repair (Review). *Front. Physiol.* **13**, 808374 (2022).

35. Walski, T. et al. Biphasic dose-response and effects of near-infrared photobiomodulation on erythrocytes susceptibility to oxidative stress in vitro. *J. Photochem. Photobiol B*. **257**, 112958 (2024).
36. Amaroli, A. et al. Photobiomodulation with 808-nm diode laser light promotes wound healing of human endothelial cells through increased reactive oxygen species production stimulating mitochondrial oxidative phosphorylation. *Lasers Med. Sci.* **34** (3), 495–504 (2019).
37. Peña, O. A. & Martin, P. Cellular and molecular mechanisms of skin wound healing. *Nat. Rev. Mol. Cell Biol.* **25** (8), 599–616 (2024).
38. Keshri, G. K. et al. Photobiomodulation with Pulsed and Continuous Wave Near-Infrared Laser (810 nm, Al-Ga-As) Augments Dermal Wound Healing in Immunosuppressed Rats. *PLoS One*. **11** (11), e0166705 (2016).
39. Chung, H. et al. The nuts and bolts of low-level laser (light) therapy. *Ann. Biomed. Eng.* **40** (2), 516–533 (2012).
40. Fukushima-Nomura, A. et al. An unbiased tissue transcriptome analysis identifies potential markers for skin phenotypes and therapeutic responses in atopic dermatitis. *Nat. Commun.* **16** (1), 4981 (2025).
41. Ryu, H. S. et al. Influence of age and regional differences on skin elasticity as measured by the Cutometer. *Skin. Res. Technol.* **14** (3), 354–358 (2008).
42. Mrówczyński, W., Mierzejewska-Krzyżowska, B. & Rosicka, K. *Skin biomechanical and viscoelastic properties measured with MyotonPRO in different areas of human body* Vol. 28, p. 236–245 (Skin Research & Technology, 2022). 2.
43. Hergesell, K. et al. The effect of long-term cigarette smoking on selected skin barrier proteins and lipids. *Sci. Rep.* **13** (1), 11572 (2023).
44. De Decker, I. et al. Influence of Moisturizers on Skin Microcirculation: An Assessment Study Using Laser Speckle Contrast Imaging. *J. Personalized Med.* **13** (10), 1507 (2023).
45. Engebretsen, K. A. et al. The effect of environmental humidity and temperature on skin barrier function and dermatitis. *J. Eur. Acad. Dermatol. Venereol.* **30** (2), 223–249 (2016).
46. Goodyear, M. D., Krleza-Jeric, K. & Lemmens, T. *The declaration of Helsinki*. *Br. Med. J. Publishing Group.* pp. 624–625. (2007).
47. Walji, S. D., Bruder, M. R. & Aucoin, M. G. Virus matrix interference on assessment of virucidal activity of high-touch surfaces designed to prevent hospital-acquired infections. *Antimicrob. Resist. Infect. Control*. **10** (1), 133 (2021).
48. Adabi, S. et al. Universal in vivo Textural Model for Human Skin based on Optical Coherence Tomograms. *Sci. Rep.* **7** (1), 17912 (2017).
49. Lenasi, H. & Strucl, M. Effect of regular physical training on cutaneous microvascular reactivity. *Med. Sci. Sports Exerc.* **36** (4), 606–612 (2004).
50. Soares, R. G. et al. Treatment of mucositis with combined 660-and 808-nm-wavelength low-level laser therapy reduced mucositis grade, pain, and use of analgesics: a parallel, single-blind, two-arm controlled study. *Lasers Med. Sci.* **33** (8), 1813–1819 (2018).
51. Menezes, S. et al. Non-coherent near infrared radiation protects normal human dermal fibroblasts from solar ultraviolet toxicity. *J. Invest. Dermatol.* **111** (4), 629–633 (1998).
52. Ronneberger, O., Fischer, P. & Brox, T. *U-Net: Convolutional Networks for Biomedical Image Segmentation. in Medical Image Computing and Computer-Assisted Intervention – MICCAI 2015* (Springer International Publishing, 2015).
53. Kepp, T. et al. Segmentation of mouse skin layers in optical coherence tomography image data using deep convolutional neural networks. *Biomedical Opt. Express*. **10** (7), 3484–3496 (2019).
54. Ibtehaz, N. & Rahman, M. S. MultiResUNet: Rethinking the U-Net architecture for multimodal biomedical image segmentation. *Neural Netw.* **121**, 74–87 (2020).

Figures

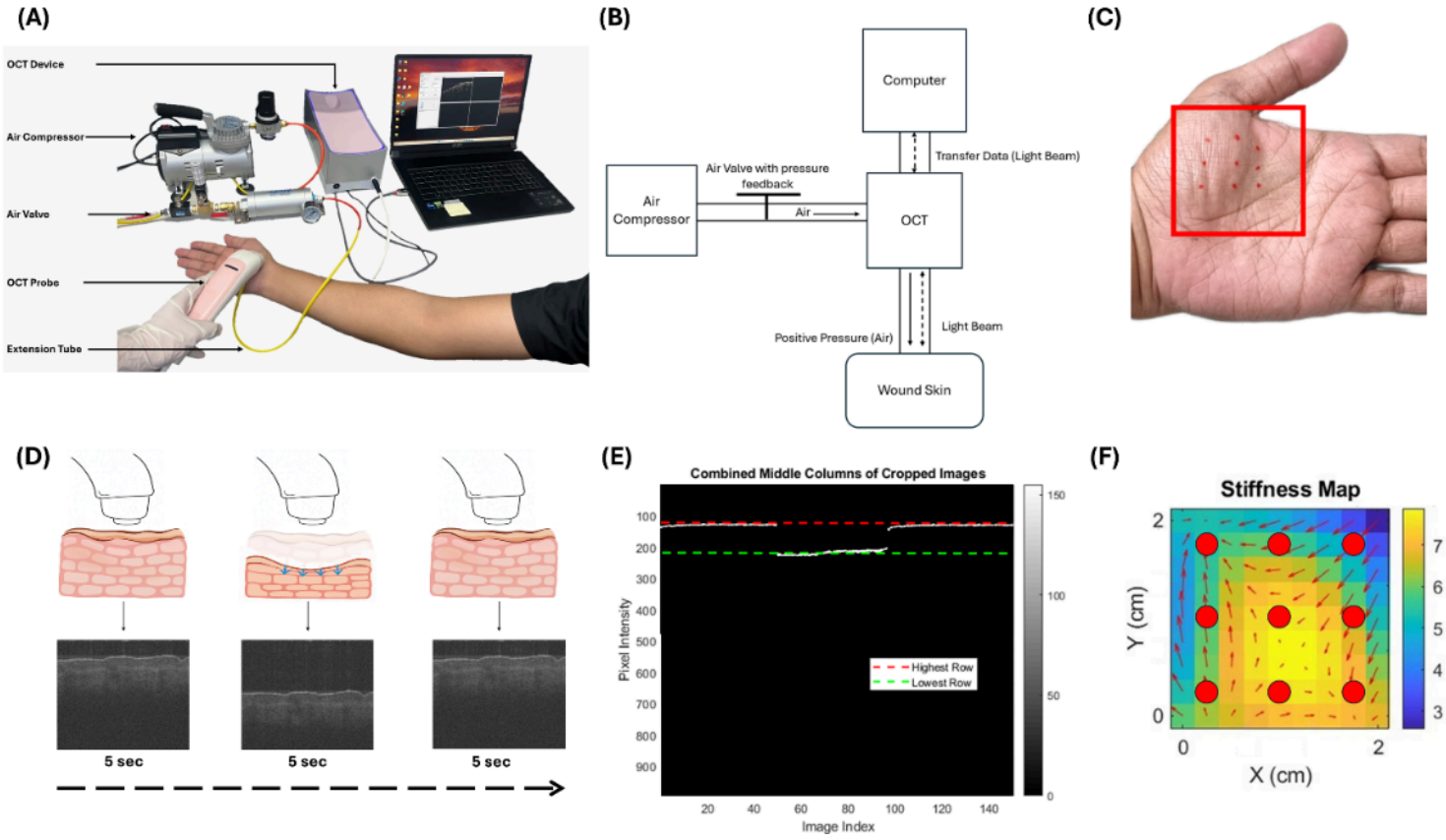


Figure 1

Overview of the fully integrated OCT. (A) OCT-air-jet indentation system; (B) Integration of Air valve and compressor procedure in OCT; (C) Measurement Location in subject; (D) Illustration of skin movement measurement with OCT in sequence time; (E) Extractions of time-lapse skin movement using deep learning; (F) Stiffness Diagram Map. *OCT, Optical Coherence Tomography.*

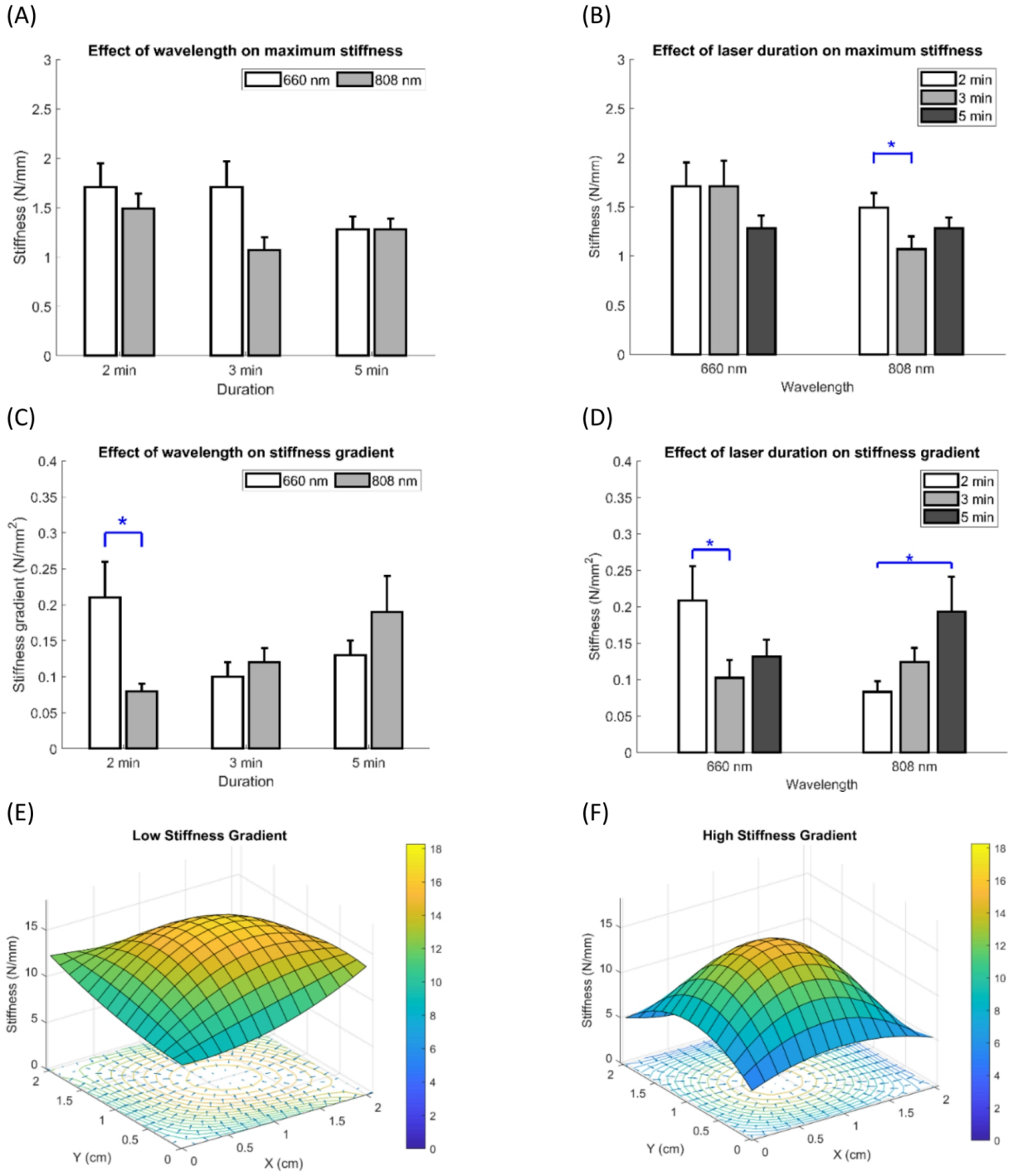


Figure 2

Effect of laser wavelength on Skin Stiffness maximum and Stiffness Gradient. (a) Effect of wavelength on maximum stiffness in different durations; (b) Effect of wavelength on stiffness gradient in different durations; (c) Effect of duration on maximum stiffness in different wavelengths; (d) Effect of duration on stiffness gradient in different wavelengths; (e) Illustration of skin stiffness with low stiffness gradient; (f) Illustration of skin stiffness with high stiffness gradient. *Data is shown as mean ± standard errors; * a significant difference (P < 0.05); N, Newton; mm, millimeter; cm, centimeter.*

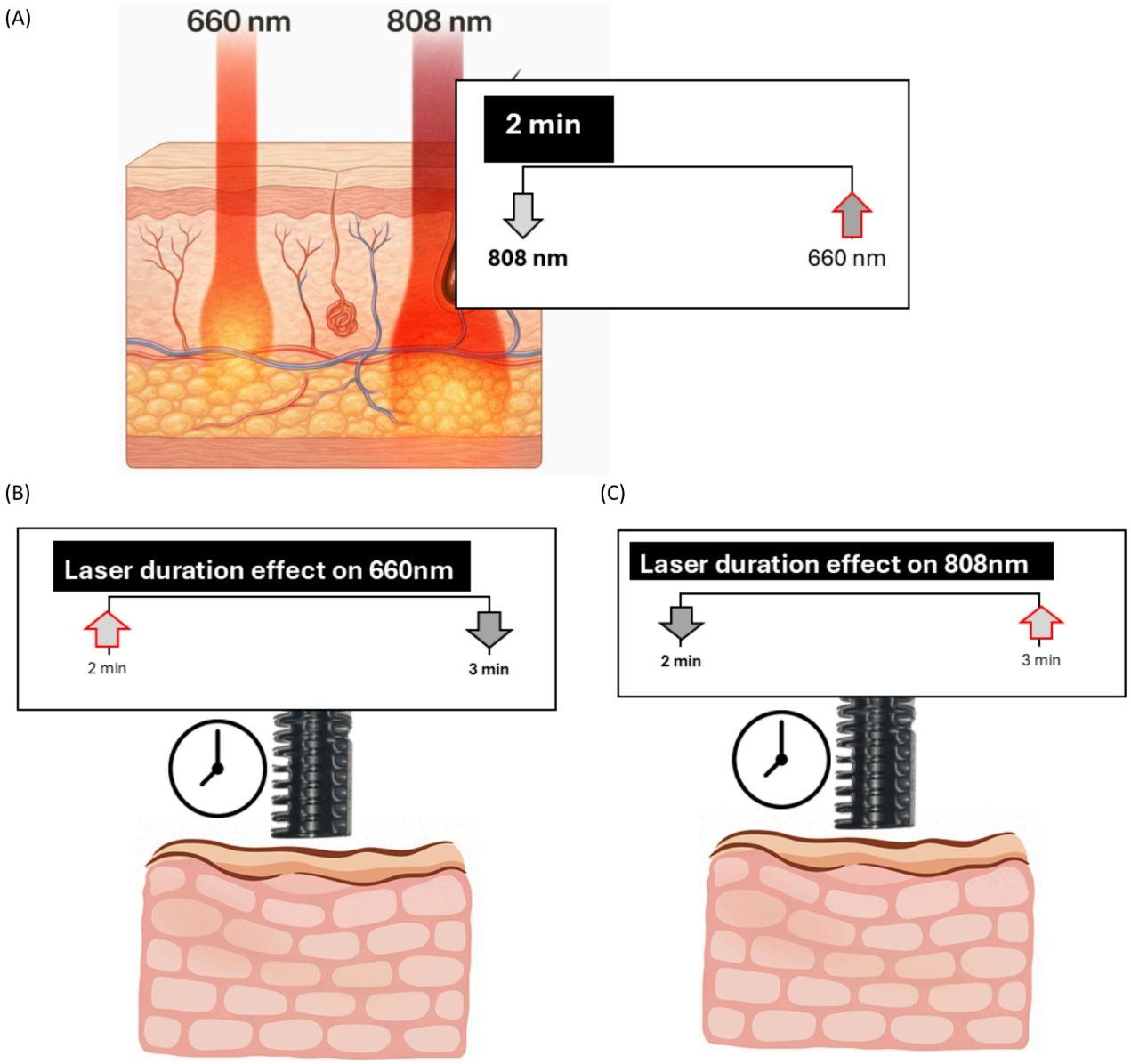


Figure 3

Illustration of the effect of the LLLT. (a) Illustration effect of the laser wavelength on skin stiffness gradient; (b) Illustration effect of the LLLT duration on skin stiffness gradient on 660 nm wavelength; (c) Illustration effect of the LLLT duration on skin stiffness gradient on 808 nm wavelength. LLLT, Low-level laser Therapy.